JACS
JOURNAL OF THE AMERICAN CHEMICAL SOCIETY
Article
pubs.acs.org/JACS

Construction of Covalent Organic Nanotubes by Light-Induced Cross-Linking of Diacetylene-Based Helical Polymers

Kaho Maeda,[†] Liu Hong,[†,‡] Taishi Nishihara,[†,‡] Yusuke Nakanishi,[†] Yuhei Miyauchi,[†,‡,§] Ryo Kitaura,[†] Naoki Ousaka,[∥] Eiji Yashima,[∥] Hideto Ito,*[,†] and Kenichiro Itami*[,†,‡,⊥]

[†]Graduate School of Science, Nagoya University, Chikusa, Nagoya 464-8602, Japan
[‡]JST-ERATO, Itami Molecular Nanocarbon Project, Nagoya University, Chikusa, Nagoya 464-8602, Japan
[§]Institute of Advanced Energy, Kyoto University, Uji, Kyoto 611-0011, Japan
[∥]Graduate School of Engineering, Nagoya University, Chikusa, Nagoya 464-8601, Japan
[⊥]Institute of Transformative Bio-Molecules (WPI-ITbM), Nagoya University, Chikusa, Nagoya 464-8602, Japan

Supporting Information

ABSTRACT: Organic nanotubes (ONTs) are tubular nanostructures composed of small molecules or macromolecules that have found various applications including ion sensor/channels, gas absorption, and photovoltaics. While most ONTs are constructed by self-assembly processes based on weak noncovalent interactions, this unique property gives rise to the inherent instability of their tubular structures. Herein, we report a simple "helix-to-tube" strategy to construct robust, covalent ONTs from easily accessible poly(*m*-phenylene diethynylene)s (poly-PDEs) possessing chiral amide side chains that can adopt a helical conformation through hydrogen-bonding interactions. The helically folded poly-PDEs subsequently undergo light-induced cross-linking at longitudinally aligned 1,3-butadiyne moieties across the whole helix to form covalent tubes (ONTs) both in solution and solid phases. The structures of poly-PDEs and covalent ONTs were characterized by spectroscopic analyses, diffraction analysis, and microscopic analyses. We envisage that this simple yet powerful "helix-to-tube" strategy will generate a range of ONT-based materials by introducing functional moieties into a monomer.

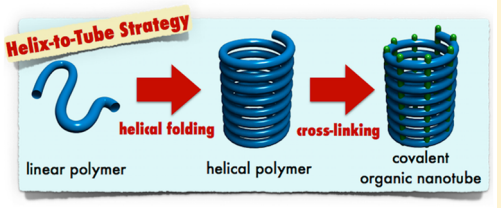

INTRODUCTION

Nanoporous materials such as metal−organic frameworks (MOFs)[1] and covalent organic frameworks (COFs)[2] have changed the landscape of nanomaterials science, and thus considerable efforts have been made in the past few decades for the design and synthesis of 2D- and 3D-nanoporous materials with diverse properties and applications. Among these materials, organic nanotubes (ONTs), which are tubular organic frameworks with a nanometer-sized cavity, have attracted much attention.[3] Arising from their unique properties such as molecular recognition, capture, release, and storage abilities,[3] ONTs are applied to host−guest chemistry, transmembrane ion channel/sensors,[4] gas absorption materials, electroconductive materials,[5] organic photovoltaics,[6] and reaction fields.[3] Conventionally, the tubular frameworks of ONTs are constructed by the self-assembly of macrocyclic molecules,[4] wedge-shaped molecules,[7] or amphiphilic molecules[5−8] based on weak noncovalent interactions such as hydrogen-bonding, $\pi-\pi$ stacking, and hydrophobic interactions (Figure 1a).[3] While these noncovalent ONTs are easily constructed, their frameworks are relatively fragile due to the weak noncovalent interactions that are used to maintain their tubular structures. In addition, the tubular frameworks are highly sensitive to solvents, pH, temperature, and many other external factors.[3]

One way to overcome the instability of noncovalent ONTs is to build stable, covalent ONTs,[9] whose tubular skeletons are cross-linked by covalent bonding (Figure 1b). This is envisaged to improve the ONTs' mechanical strength, thermal stability, and carrier mobility, as well as to impart additional electrochemical, photophysical, and spintronic properties. While the general synthetic strategy for covalent ONTs is yet to be established, the construction of covalent ONTs has been attempted by the cross-linking of macrocyclic components in noncovalent ONTs.[9,10] For example, Morin[9d,e] reported the synthesis of covalent ONTs using topochemical polymerization[11] of macrocylic *m*-phenylene diethynylene in the gel state. Although this work represents a significant breakthrough in covalent ONT synthesis, there are several drawbacks, such as the difficulties in the synthesis of macrocyclic components and in the achievement of a suitable tubular conformation for the cross-linking reaction from the crystallization or self-assembly of macrocyclic components in the solid or gelatinous states.[9,10] To advance the science of covalent ONTs, we decided to focus on establishing a general, reliable, and versatile synthetic strategy for covalent ONTs, which should open a new vista of a range of ONT applications.

Received: June 9, 2016
Published: August 3, 2016

DOI: 10.1021/jacs.6b05582
J. Am. Chem. Soc. 2016, 138, 11001−11008

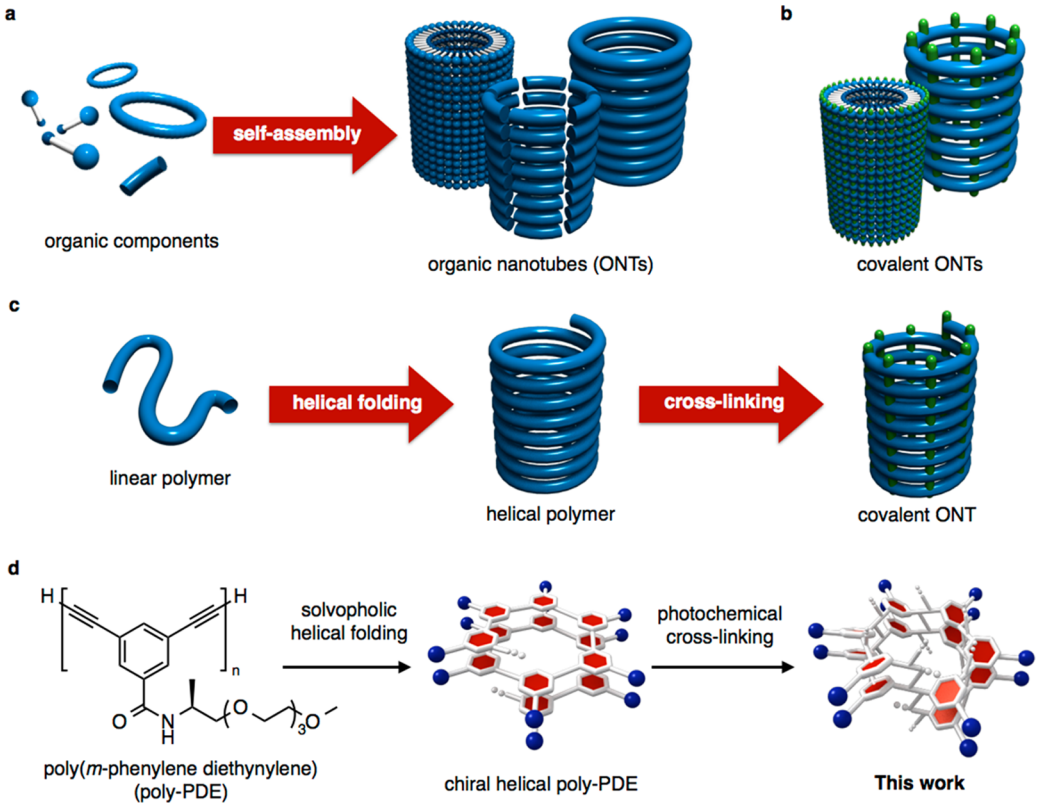

Figure 1. Synthetic strategies toward noncovalent and covalent ONTs. (a) Well-established synthetic strategies toward noncovalent ONTs by self-assembling of amphiphilic molecules, wedge-shaped molecules, and macrocyclic molecules. (b) Covalent ONTs derived from noncovalent ONTs by cross-linking. (c) Current synthetic approach toward covalent ONTs through longitudinal cross-linking between helical pitches in helical polymers. (d) Helically folded poly(*m*-phenylene diethynylene) (poly-PDE) bearing chiral amide side chains and photochemical cross-linking between longitudinal diacetylenes (this work).

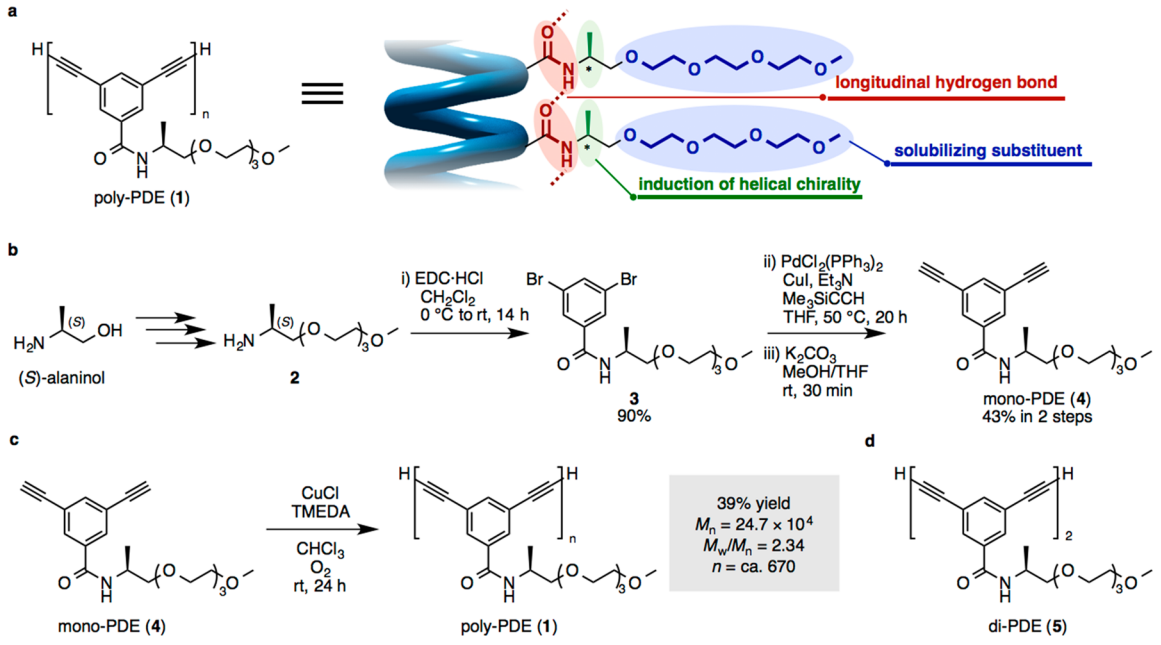

Figure 2. Design and synthesis of poly-PDE (**1**). (a) Molecular design for helical poly-PDE bearing chiral amide side chains (**1**). (b) Synthetic scheme for 3,5-diethynylbenzamide bearing a chiral amide side chain (mono-PDE, **4**) as a monomer for poly-PDE (**1**). Reaction conditions: (i) **2** (1.1 equiv), EDC·HCl (1.1 equiv), (*S*)-alaninol (1.0 equiv), CH_2Cl_2, rt, 14 h, 90%; (ii) **3** (1.0 equiv), trimethylsilylacetylene (2.2 equiv), $PdCl_2(PPh_3)_2$ (8 mol %), CuI (5 mol %), Et_3N (3.0 equiv), THF, 50 °C, 20 h, 61%; (iii) K_2CO_3 (1.0 equiv), MeOH/THF, rt, 30 h, 70%. EDC = *N*-[3-(dimethylamino)propyl]-*N*′-ethylcarbodiimide. (c) Synthesis of poly-PDE (**1**) by polymerization of mono-PDE (**4**) through copper-catalyzed Glaser–Hay coupling. (d) Structure of di-PDE (**5**).

DOI: 10.1021/jacs.6b05582
J. Am. Chem. Soc. 2016, 138, 11001–11008

We envisioned that covalent ONTs could be easily constructed from helically folded polymers by the cross-linking at longitudinally repeating pitches (Figure 1c).[12] With this "helix-to-tube" strategy, we further contemplated that poly(*m*-phenylene diethynylene)s (poly-PDEs)[13] and the photochemical reaction (topochemical polymerization[11]) of diynes would be applicable as a helical polymer and cross-linking reaction, respectively (Figure 1d). Since the ground-breaking discovery of helix-forming *m*-phenylene ethynylene oligomers by Moore and co-workers in 1997,[14] a number of studies on the synthesis and structural analysis of helical poly(arylene ethynylene)s and poly(arylene diethynylene)s have been reported.[13−15] To date, a series of arylene ethynylene polymers are regarded as one of the most established motifs for helix-forming polymers. We have also reported the synthesis of amphiphilic poly(*m*-phenylene ethynylene)s (poly-PEs) bearing chiral amide side chains, and revealed their chiral helical folding behavior by hydrogen-bonding in solution.[15] Furthermore, X-ray diffraction (XRD) analysis and atomic force microscopy (AFM) measurement clarified their self-assembling images, helical senses, and the distance between helical pitches. These findings led us to use poly-PDE, an analogue of poly-PE having a 1,3-butadiyne unit, as a promising precursor for the construction of covalent ONTs.

RESULTS AND DISCUSSION

Design and Synthesis of Helical Polymer. We initiated our studies by the rational design and synthesis of helical poly-PDE **1** having chiral alkylamide side chains (Figure 2a). On the basis of the previous report on poly-PE bearing the same chiral amide pendant,[15] poly-PDE **1** is expected to form a stable helical conformation by the N−H−O hydrogen bonds between longitudinally adjacent side chains. Furthermore, chiral amide moieties would induce the formation of a one-handed helix of **1** (*helix*-**1**), which should allow the easy verification of helix formation by simple circular dichroism (CD) measurement. The oligoethylene glycol moiety on the termini of side chains is expected to improve the solubility of both poly-PDE and the target covalent ONTs in organic solvents to simplify the handling and analysis of these compounds. On the basis of these molecular designs, we synthesized poly-PDE **1** as shown in Figure 2b. The condensation of 3,5-dibromobenzoic acid with chiral amine **2**[15] (derived from (*S*)-2-amino-1-propanol), followed by the Sonogashira coupling with trimethylsilylacetylene, and subsequent deprotection of the silyl group successfully afforded 3,5-diethynylbenzamide **4** as a monomer (mono-PDE) for poly-PDE **1**. After extensive investigation of the suitable conditions to polymerize mono-PDE **4**, we found that the Glaser−Hay coupling conditions with catalytic CuCl and *N*,*N*,*N*′,*N*′-tetramethylethylenediamine (TMEDA) in $CHCl_3$ under an O_2 atmosphere converted **4** into high-molecular-weight poly-PDE **1** (Figure 2c). After purification by size exclusion chromatography (SEC), the yellow solid was obtained in 39 wt % yield. With SEC analysis with polystyrene standards, the number-average molecular weight (M_n) and polydispersity index (M_w/M_n) were estimated to be 2.5×10^5 and 2.3, respectively. The polymerization degree (n) based on M_n was calculated to be approximately 670. The dimer of **1** (di-PDE **5**) was also synthesized for spectroscopic comparison (Figure 2d).

Spectroscopic Analyses of Poly-PDE. We subsequently analyzed the photophysical and chiroptical properties of poly-PDE **1** to evaluate its helical folding behavior. As summarized in Figure 3a, poly-PDE **1** was found to form a chiral helix structure (*helix*-**1**) in $CHCl_3$, CH_2Cl_2, tetrahydrofuran (THF),

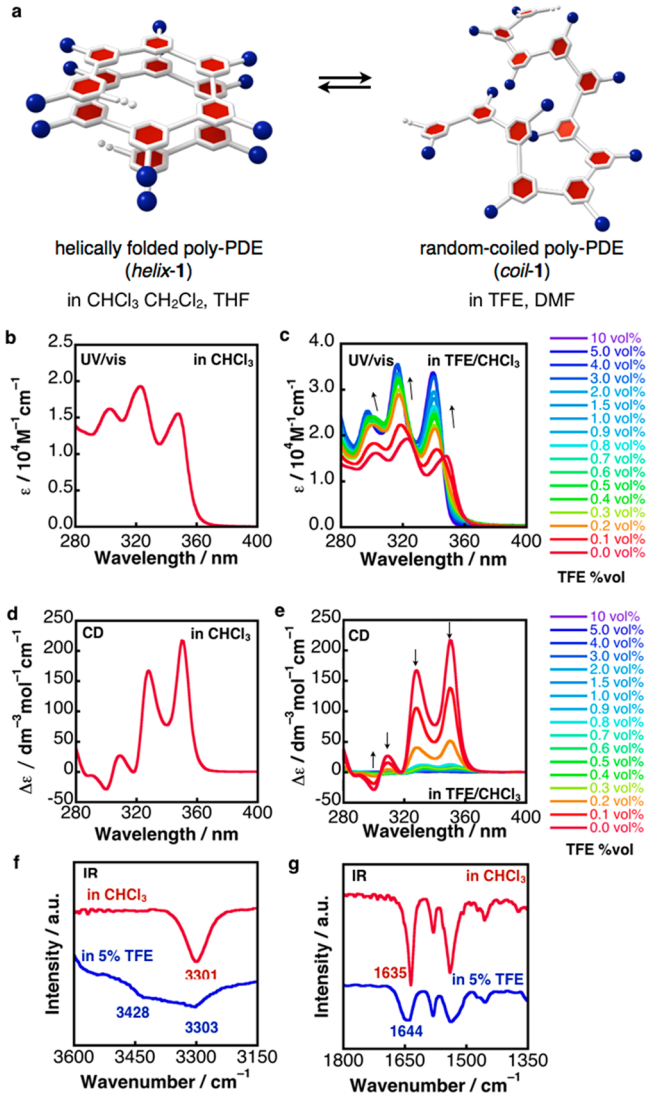

Figure 3. Spectroscopic analyses of poly-PDE (**1**). (a) Conformational changes of poly-PDE (**1**) correspond to chiral helical structure (*helix*-**1**) in $CHCl_3$, CH_2Cl_2, and THF, and random-coiled structure (*coil*-**5**) in TFE and DMF. TFE = 2,2,2-trifluoroethanol. DMF = *N*,*N*′-dimethylformamide. (b) UV−vis absorption spectrum of poly-PDE (**1**) in $CHCl_3$. (c) Spectral changes in UV−vis absorption spectra of poly-PDE (**1**) with increasing vol % of TFE in $CHCl_3$. (d) CD spectrum of poly-PDE (**1**) in $CHCl_3$. (e) Spectral changes in CD spectra of poly-PDE (**1**) with increasing vol % of TFE in $CHCl_3$. (f) IR spectra of poly-PDE (**1**) in $CHCl_3$ (red line) and TEF/$CHCl_3$ (blue line) in the range around 3300 cm^{-1}. (g) IR spectra of poly-PDE (**1**) in $CHCl_3$ (red line) and TEF/$CHCl_3$ (blue line) in the range around 1600 cm^{-1}.

and methanol, and an achiral random-coil structure (*coil*-**1**) in 2,2,2-trifluoroethanol (TFE) and *N*,*N*′-dimethylformamide (DMF) (*vide infra* and see Figures S3 and S4 in the Supporting Information (SI) for detailed discussion). In the UV−vis absorption spectrum of poly-PDE **1** in $CHCl_3$ (*helix*-**1**), three absorption maxima were found at 303, 323, and 348 nm (Figure 3b). In the CD spectrum of poly-PDE **1** in $CHCl_3$ (*helix*-**1**), strong positive Cotton effects were observed at 328 and 350 nm (Figure 3d). This result was quite similar to the

DOI: 10.1021/jacs.6b05582
J. Am. Chem. Soc. 2016, 138, 11001−11008

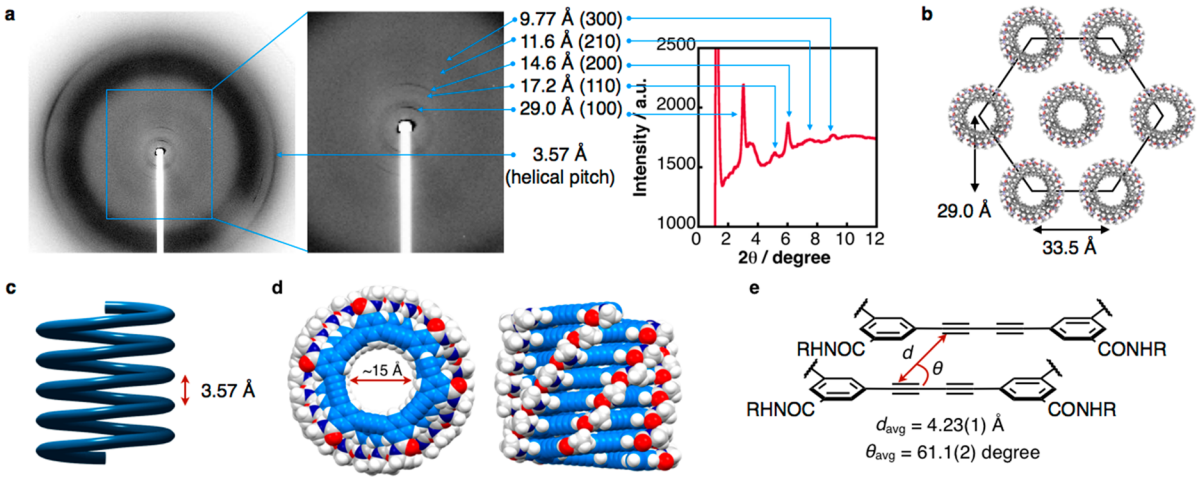

Figure 4. Structural analyses by wide-angle X-ray diffraction (WAXD) of helical poly-PDE (*helix*-**1**) in the solid state. (a) WAXD patterns of magnetically oriented film of *helix*-**1** prepared from concentrated $CHCl_3$ solution. (b) Schematic illustration of a possible hexagonal packing of *helix*-**1**. Terminal substituents on amide side chains are omitted for clarity. (c) Schematic illustration of *helix*-**1** having 3.57 Å of helical pitch confirmed by diffraction pattern of WAXD. (d) Optimized structure of *helix*-**1** in a top view (left) and a side view (right) on the basis of XRD structural analyses followed by molecular mechanics calculations (see SI). *N*-Methylamide was used as side chains for the model of *helix*-**1**, which are shown using the space-filling model. (e) Average distance (d_{avg}) and angle (θ_{avg}) between longitudinally aligned diacetylenes in the optimized molecular model.

previous reports on a series of helical foldamers.[15] In addition, the UV−vis absorption and CD spectra of di-PDE **5** were measured for comparison (Figures S15 and S16 in SI). Cotton effects were not observed in the $CHCl_3$ solution of di-PDE **5** (Figure S16 in SI), which indicates that the observed Cotton effects with *helix*-**1** were attributed to neither a chiral carbon center of amide side chain nor the intermolecular chiral assembly, but to the helical chirality of the whole polymer. Significant spectral changes in the absorption spectra of *helix*-**1**, namely, the blue-shift and the hyperchromic effect, were observed by the addition of TFE to the $CHCl_3$ solution (Figure 3c). These phenomena could be considered as the outcome of the breaking of hydrogen bonds, the helical conformation, and $\pi-\pi$ stacking between benzamide moieties to form an achiral random-coiled structure (*coil*-**1**).[16]

When TFE was added to the solution of **1** in $CHCl_3$, a dramatic decrease in the Cotton effects was also observed (Figure 3e), and the addition of only 0.3 vol % of TFE was found to be sufficient to unfold the chiral helix (Figure 3e and Figures S9−S12). In the FT-IR spectrum of *helix*-**1** in $CHCl_3$, strong peaks were observed at 3301 and 1635 cm^{-1}, which could be assigned to the N−H and C−O stretching vibration modes, respectively (Figure 3f,g). These peaks were quite similar to those of poly-PEs bearing the same chiral amide pendants.[15] These results imply that the helical conformation of *helix*-**1** was stabilized by the intramolecular hydrogen bonds between longitudinally adjacent amide side chains. When 5 vol % of TFE was added to the solution of **1** in $CHCl_3$, intense peaks corresponding to the stretching vibration of hydrogen-bonding C−O and N−H were broadened, and higher wavenumber-shifted peaks of 3428 and 1644 cm^{-1} newly emerged, although hydrogen-bonding amide N−H stretching vibrations still remained to some extent (Figure 3f,g). Overall, it was evident that unwrapping of the helical structure (*helix*-**1**) to the random-coiled structure (*coil*-**1**) was triggered by acid-mediated cleavage of the hydrogen bonds.[15]

Helix Formation of Poly-PDE in the Solid State. For achievement of the photochemical cross-linking (topochemical polymerization) of 1,3-butadiynes in *helix*-**1**, the alignment of diynes was of critical importance. Therefore, we carried out the structural analyses of *helix*-**1** in the solid state by wide-angle X-ray diffraction (WAXD). A sample film of magnetically oriented *helix*-**1** was prepared following previous reports[15,17] (Figure S17 in SI). In the WAXD measurement, some arc-shaped reflection patterns were observed in the meridional and equatorial regions (Figure 4a). Five meridional reflections were observed at 29.0, 17.2, 14.6, 11.6, and 9.77 Å, which could be assigned as the reflection patterns in the 2D hexagonal lattice of a = 33.5 Å (Figure 4b). This lattice value was larger by 2−3 Å than those in poly-PEs reported by Moore[18] and our group,[15] which was in line with the helix containing longer 1,3-butadiyne units. Furthermore, intense reflections were found at 3.57 Å, which corresponds to the helical pitch distance between benzamide moieties (Figure 4c). This result was almost the same as the corresponding helical pitches and $\pi-\pi$ stacking distances between benzene rings in reported poly-PEs.[15] On the basis of the obtained data from WAXD analysis, we optimized the structure of *helix*-**1** by using molecular mechanics calculations of 40-mer of poly-PDE bearing simple *N*-methylamide pendants (Figure 4d and Figure S18 in SI). The optimized structure was obtained by taking into account the typical value of 1.7−1.9 Å for the hydrogen bonds of amides between the helical pitches, 3.57 Å for the helical pitch, and the hypothesis that the polymer has ∼6 monomer units in one helical turn[15,19] (Figure S18 in SI). The average distance between longitudinally aligned 1,3-butadiynes (d) and their average angle (θ) were estimated to be 4.23(1) Å and 61.1(2)°, respectively (Figure 4e, Figure S18, and Table S1). These values were within the range of appropriate d (4−6 Å) and θ (40−65°) in the general topochemical polymerization of 1,3-diynes in the solid state.[11b]

We further investigated the structural analysis of *helix*-**1** by atomic force microscopy (AFM) measurements on a highly oriented pyrolytic graphite (HOPG) substrate. The sample on a HOPG substrate was prepared by the drop-casting of a 0.02 mg mL^{-1} solution of **1** in degassed $CHCl_3$ onto the freshly exfoliated HOPG, followed by evaporation at room temperature for 1.5 h *in vacuo*. Figure 5a shows an uneven pattern of oriented *helix*-**1** in a height image with a constant height of 2.8

DOI: 10.1021/jacs.6b05582
J. Am. Chem. Soc. 2016, 138, 11001−11008

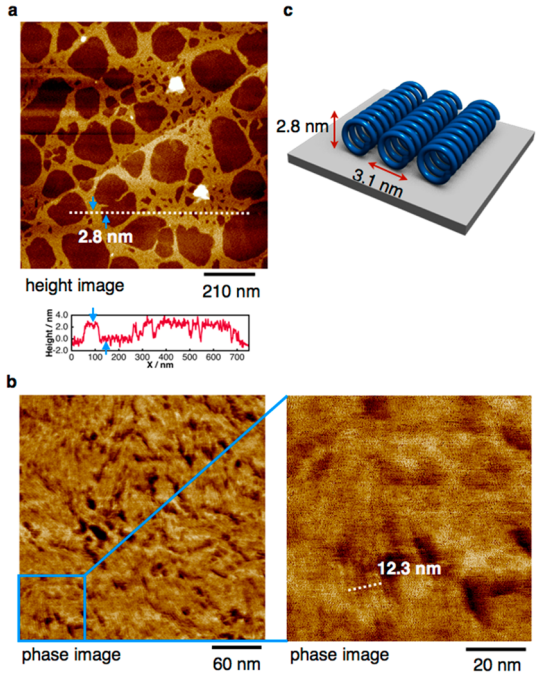

Figure 5. AFM measurements of helical poly-PDE (*helix*-**1**) in the solid state. (a) Height and (b) phase images on a HOPG substrate prepared by casting the solution of *helix*-**1** in $CHCl_3$ at 25 °C. (c) Schematic illustration of aligned *helix*-**1** having a height of 2.8 nm and a width of 3.1 nm on a HOPG substrate.

nm. The obtained height was reasonable for the 2D helix-bundles of *helix*-**1**, and was slightly larger than the height of 2.6 nm[15] observed for poly-PEs in AFM measurements. Equally spaced stripe patterns were also observed in the phase image, and the bundled four stripes with a 12.3 nm width marked with a white broken line were distinguishable (Figure 5b). The width per stripe was estimated to be 3.1 nm, which was approximately identical to the outer diameter of *helix*-**1** (Figure 5c). These results indicate that the helical structure of *helix*-**1** was sustained not only in solution but also in the solid state.

Photochemical Cross-Linking in Helically Folded Poly-PDE. Having confirmed the helix structure of poly-PDE **1**, we performed the cross-linking of helical poly-PDE **1** by light irradiation in both solution and solid states (Figure 6a). First, a degassed solution of *helix*-**1** in $CHCl_3$ (1.0 mg mL^{-1}) was irradiated at room temperature under a N_2 atmosphere with a 100-W high-pressure Hg lamp, and the reaction progress was monitored by Raman spectroscopy (Figure 6b and Figure S20 in SI). For comparison, the reactions of *coil*-**1** in 5 vol % TFE/$CHCl_3$, DMF and di-PDE **5** in $CHCl_3$ were also conducted under otherwise identical conditions (Figure 6c and Figures S23–S25 in SI). In all cases, the peaks of conjugated diyne moieties of starting materials around 2200 cm^{-1} disappeared after 1 h of irradiation. The reaction of *helix*-**1** showed the emergence of distinct peaks at 2109, 1467, and 1412 cm^{-1}, which may be derived from the desired covalent ONT **6** (Figure 6b). The reactions of *coil*-**1** in TFE/$CHCl_3$, DMF and di-PDE **5** in $CHCl_3$ resulted in only the disappearance of starting materials (Figure 6c and Figures S23–S25 in SI). These reactions were likely to have produced a complex mixture by intra- and intermolecular random cross-linking or decomposition.[20] The new peaks at 2109, 1467, and 1412 cm^{-1} observed in the reaction of *helix*-**1** were consistent with the stretching vibrations of acetylene (around 2100 cm^{-1}) and

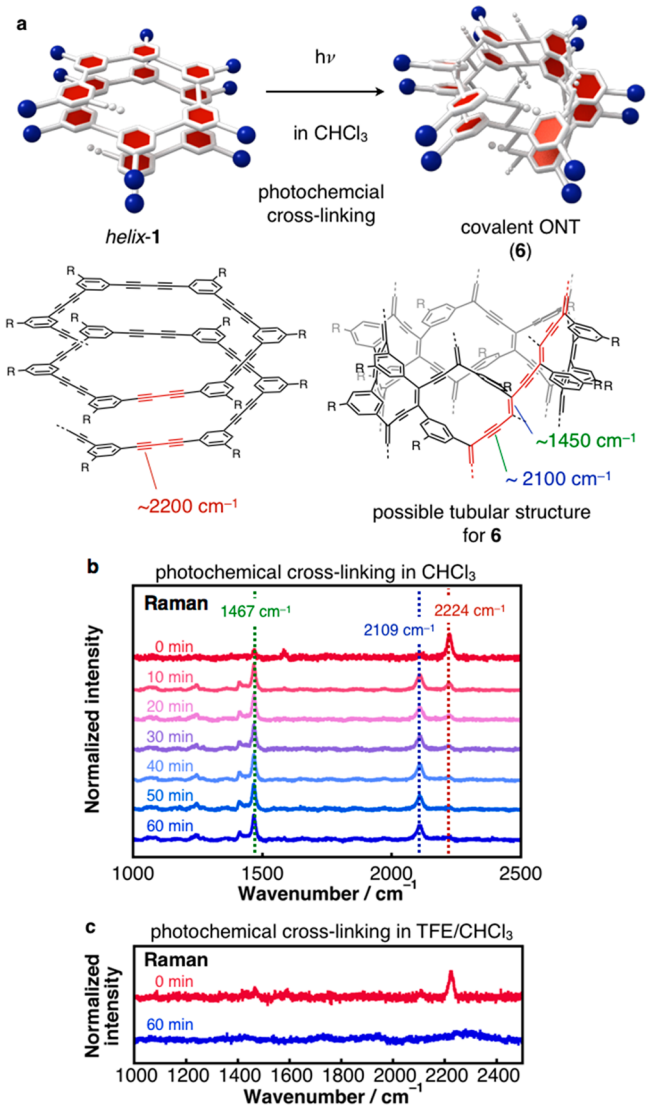

Figure 6. Photochemical cross-linking of *helix*-**1**, and Raman spectroscopic analyses of the reaction and covalent ONT **6**. (a) Schematic illustration of photochemical cross-linking of *helix*-**1** for the synthesis of covalent ONT **6**. Indicated wavenumbers in structures of *helix*-**1** and **6** correspond to general Raman peaks observed in 1,3-butadiyne and enyne substructures of polydiacetylenes. (b) Changes in Raman spectra for the photochemical cross-linking of *helix*-**1** in $CHCl_3$ under light irradiation by a 100-W high-pressure Hg lamp. Raman spectra were measured using a 633 nm excitation laser with intensity of 16 mW/cm^2. (c) Changes in Raman spectra by the irradiation of *coil*-**1** in 5 vol % TFE/$CHCl_3$ with a 100-W high-pressure Hg lamp. Raman spectra were measured using a 633 nm excitation laser with the intensity of 16 mW/cm^2.

alkene (around 1450 cm^{-1}) in the conjugated enyne moieties[11e,21] of the cross-linked structure in **6**.

To prove the formation of the covalent ONT, we further collected spectroscopic data such as UV–vis absorption and emission spectra (Figure 7). It was found during these studies that the photochemical cross-linking of *helix*-**1** proceeded even under irradiation of excitation light in a fluorescence spectrophotometer, although at a slower rate. This allowed us to monitor the reaction progress under the irradiation of the degassed $CHCl_3$ solution of poly-PDE **1** at 365 nm excitation. Upon completion of the reaction after 81 h, the UV–vis absorption spectrum of the product clearly showed the

DOI: 10.1021/jacs.6b05582
J. Am. Chem. Soc. 2016, 138, 11001–11008

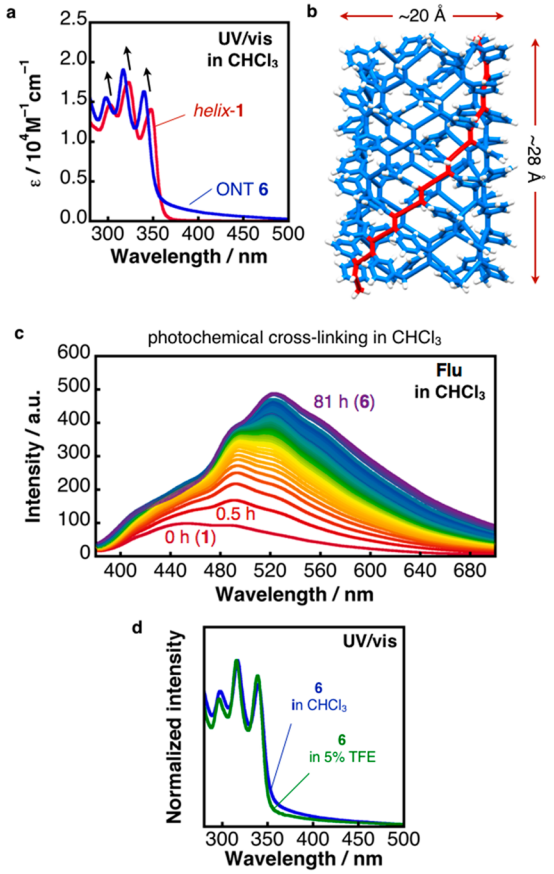

Figure 7. Spectral changes in photochemical cross-linking of *helix*-**1**. (a) UV−vis absorption spectra of *helix*-**1** (red line) and ONT **6** (blue line). (b) Optimized molecular model of ONT **6** composed of 48 monomer units. Amide substituents and tube termini are replaced with hydrogen atoms for optimization. One polydiacetylene substructure is highlighted with a red line. (c) Time-dependent changes of fluorescence spectra in photochemical cross-linking of *helix*-**1** in $CHCl_3$ at under irradiation of excitation light at 365 nm in a fluorescence spectrophotometer. (d) Absorption spectra of ONT **6** in $CHCl_3$ (blue line) and in 5 vol % TFE/$CHCl_3$ (green line).

following changes: broadened shoulder absorption peaks from 350 to 500 nm appeared, and three absorption maxima were blue-shifted to 340, 317, and 298 nm (Figure 7a). Shoulder peaks at the longer wavelength region clearly indicated the formation of a conjugate polydiacetylene substructure in covalent ONT **6**. The blue-shifted absorption maxima could be considered as a result of the stark conformational changes related to the dissociation of $\pi-\pi$ stackings between benzamides. In a molecular model for the ideal covalent ONT (**6**) shown in Figure 7b, benzamide moieties were at least 4−5 Å away from longitudinally adjacent moieties, indicating the dissociation of $\pi-\pi$ stackings. We also observed time-dependent changes of fluorescence spectra during irradiation under the irradiation of 365 nm excitation light (Figure 7c and Figure S28 in SI). As the reaction proceeded, the maximum emission wavelength gradually red-shifted from 453 to 524 nm. This gradual red-shift was considered to be a typical phenomenon in the topochemical polymerization of diynes.[22] We also confirmed that the spectrum of **6** does not change even with the addition of 10 vol % TFE (Figure 7d), which was consistent with the rigid framework of covalent ONT **6**. While we had expected the maintenance of chiral framework even in ONT **6** derived from chiral helical poly-PDE (*helix*-**1**), almost no Cotton effect was observed in the CD spectrum of ONT **6** (see Figure S29). This probably means that a few defects on the cross-linking made the tube structure achiral as a whole, or chirality transfer from the chiral amide side chains is becoming less efficient with racemization occurring just prior to the cross-linking.

In the solution-phase photochemical cross-linking of *helix*-**1** (Figure 7c), emission peaks at wavelength shorter than 500 nm were still found even after 81 h, and this supports the existence of short polydiacetylene substructures by incomplete cross-linking.[23] Interestingly, the cross-linking of *helix*-**1** was found to be much faster in the solid state. A film of *helix*-**1** on a silicon substrate (prepared by the drop-casting and the slow evaporation of polymer solution) was irradiated with a 100-W Hg lamp (Figure 8a). Direct observation of Raman spectra on a

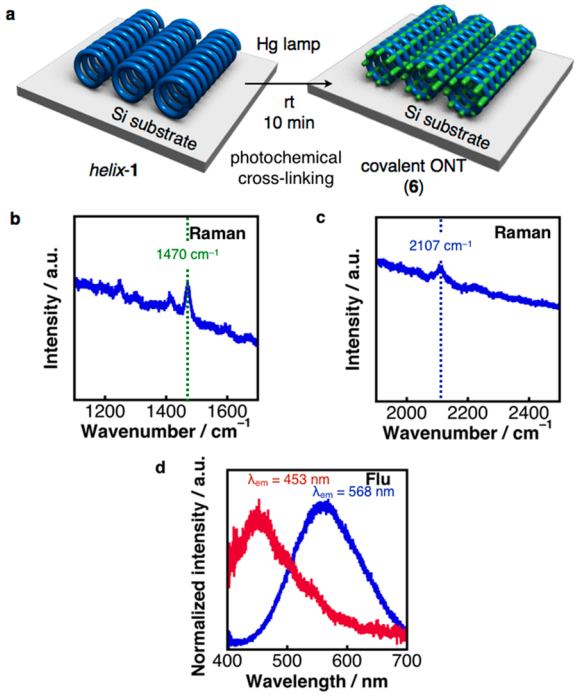

Figure 8. (a) Schematic illustration of the synthesis of ONT **6** by photochemical cross-linking of *helix*-**1** on a silicon substrate. (b) Raman spectrum around 1400 cm^{-1} of ONT **6** obtained by photochemical cross-linking on a silicon substrate. (c) Raman spectrum around 2200 cm^{-1} of ONT **6** obtained by photochemical cross-linking on a silicon substrate. (d) Solid-state fluorescence spectra (excitation wavelength = 340 nm) of poly-PDE (**1**) on a silicon substrate (red line) and ONT **6** obtained by photochemical cross-linking on a silicon substrate (blue line).

silicon substrate revealed that the reaction was completed within 10 min to generate covalent ONT **6** (Figures 8b,c). Furthermore, the product showed the emission having a single emission maximum at 570 nm without any prominent emission peak at wavelength shorter than 500 nm (Figure 8d), which also indicates the formation of covalent ONT (**6**) with a high degree of cross-linking. On the other hand, cross-linking did not proceed with *coil*-**1** on a silicon substrate (Figure S30 in SI). Consequently, as we expected, the helical conformation of poly-PDE **1** was an essential factor for the progress of photochemical cross-linking both in solution and solid phases.

DOI: 10.1021/jacs.6b05582
J. Am. Chem. Soc. 2016, 138, 11001−11008

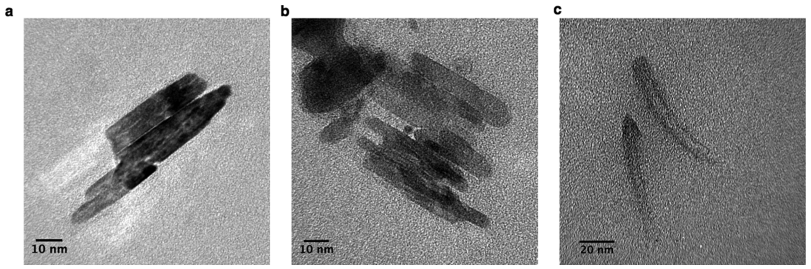

Figure 9. TEM measurements of covalent ONT **6**. (a–c) TEM images of the bundle structures of ONT **6** on a carbon-coated copper grid. ONT **6** was prepared by photochemical cross-linking of *helix*-**1** in $CHCl_3$ under the irradiation with 100-W high-pressure Hg lamp at room temperature under a N_2 atmosphere for 1 h.

TEM Measurements of Covalent ONT. Finally, the direct observation of the synthesized covalent ONT **6** by transmission electron microscopy (TEM) was examined. While aggregation and/or decomposition images of ONT **6** were observed in most of the TEM measurements, which likely reflects the molecular nature of the ONT used in our studies (Figure S31 in SI), bundles of rod-like materials were also observed (Figure 9a,b). One distinguishable rod in Figure 9a was estimated to be ca. 40–50 nm in length and ca. 4–5 nm in width. This length and width correlate to those of covalent ONT **6** derived from poly-PDE **1** composed of 670 monomer units (the tube length per monomer unit was roughly estimated to be 0.6 Å according to Figure 7b). Importantly, isolated tube-like images were observed albeit with low contrast (Figure 9c). Although further verification of the existence of the inner hollow cavity may be necessary depending on the applications of ONT in the future, the objects observed in the present TEM images do not contradict the ideal structure of ONT **6**.

CONCLUSION

In summary, we have established a simple and efficient synthetic method for covalent organic nanotubes from easily accessible diacetylene-based helical polymers. Our "helix-to-tube" strategy relies on the efficient cross-linking of 1,3-butadiyne units in the main chain of helical poly(*m*-phenylene diethynylene)s by an operationally simple light irradiation. The use of chiral side chains in the starting polymer allows easy analysis in the formation of the helical polymer and the covalent organic nanotubes. By simply changing the arene unit in monomer and the polymerization degree, our method can in principle generate various covalent organic nanotubes with designed diameters, tube lengths, and functionalities such as the molecular recognition and metal coordination abilities. Further developments of the "helix-to-tube" methodology, synthesis, and application of various covalent organic nanotubes are currently ongoing in our laboratory.

ASSOCIATED CONTENT

Supporting Information

The Supporting Information is available free of charge on the ACS Publications website at DOI: 10.1021/jacs.6b05582.

Experimental procedures and characterization data for all compounds, results of spectroscopic and microscopic measurements, and computational results for the molecular modeling (PDF)

AUTHOR INFORMATION

Corresponding Authors

*ito.hideto@g.mbox.nagoya-u.ac.jp
*itami@chem.nagoya-u.ac.jp

Notes

The authors declare no competing financial interest.

ACKNOWLEDGMENTS

This work was supported by the ERATO program from JST (K.I.), the KAKENHI from MEXT (26810057 and 16H00907 to H.I.), and a grant from SHOWA DENKO Award in Synthetic Organic Chemistry, Japan (H.I.). We thank Dr. Ayako Miyazaki for critical comments and Prof. Hisanori Shinohara for various kinds of support. Calculations were performed using the resources of the Research Center for Computational Science, Okazaki, Japan. We thank Dr. Tatsuo Hikage for wide-angle X-ray diffraction analyses in High Intensity X-ray Diffraction laboratory, Nagoya University. ITbM is supported by the World Premier International Research Center (WPI) Initiative, Japan.

REFERENCES

(1) Related study and review on metal–organic frameworks: (a) Li, H.; Eddaoudi, M.; O'Keeffe, M.; Yaghi, O. M. *Nature* **1999**, *402*, 276. (b) Kitagawa, S.; Kitaura, R.; Noro, S. *Angew. Chem., Int. Ed.* **2004**, *43*, 2334.

(2) Reviews on covalent organic frameworks: (a) Feng, X.; Ding, X.; Jiang, D. *Chem. Soc. Rev.* **2012**, *41*, 6010. (b) Ding, S.-Y.; Wang, W. *Chem. Soc. Rev.* **2013**, *42*, 548.

(3) Reviews on organic nanotubes: (a) Shimizu, T. *Bull. Chem. Soc. Jpn.* **2008**, *81*, 1554. (b) Shimizu, T. *J. Polym. Sci., Part A: Polym. Chem.* **2006**, *44*, 5137. (c) Kameta, N.; Minamikawa, H.; Masuda, M. *Soft Matter* **2011**, *7*, 4539. (d) Bakbo Block, M. A.; Kaiser, C.; Khan, A.; Hecht, S. *Top Curr. Chem.* **2005**, *245*, 89.

(4) (a) Ghadiri, M. R.; Granja, J. R.; Milligan, R. A.; McRee, D. E.; Khazanovich, N. *Nature* **1993**, *366*, 324. (b) Ghadiri, M. R.; Granja, J. R.; Buehler, L. K. *Nature* **1994**, *369*, 301. (c) Helsel, A. J.; Brown, A. L.; Yamato, K.; Feng, W.; Yuan, L.; Clements, A. J.; Harding, S. V.; Szabo, G.; Shao, Z.; Gong, B. *J. Am. Chem. Soc.* **2008**, *130*, 15784.

(5) (a) Hill, J. P.; Jin, W.; Kosaka, A.; Fukushima, T.; Ichihara, H.; Shimomura, T.; Ito, K.; Hashizume, T.; Ishii, N.; Aida, T. *Science* **2004**, *304*, 1481. (b) Yamamoto, Y.; Fukushima, T.; Suna, Y.; Ishii, N.; Saeki, A.; Seki, S.; Tagawa, S.; Taniguchi, M.; Kawai, T.; Aida, T. *Science* **2006**, *314*, 1761.

(6) Yamamoto, Y.; Zhang, G.; Jin, W.; Fukushima, T.; Ishii, N.; Saeki, A.; Seki, S.; Tagawa, S.; Minari, T.; Tsukagoshi, K.; Aida, T. *Proc. Natl. Acad. Sci. U. S. A.* **2009**, *106*, 21051.

(7) (a) Fenniri, H.; Mathivanan, P.; Vidale, K. L.; Sherman, D.; Hallenga, K.; Wood, K. V.; Stowell, J. G. *J. Am. Chem. Soc.* **2001**, *123*, 3854. (b) Kimizuka, N.; Kawasaki, T.; Hirata, K.; Kunitake, T. *J. Am. Chem. Soc.* **1995**, *117*, 6360. (c) Huang, Z.; Kang, S.-K.; Banno, M.;

DOI: 10.1021/jacs.6b05582
J. Am. Chem. Soc. 2016, 138, 11001–11008

Yamaguchi, T.; Lee, D.; Seok, C.; Yashima, E.; Lee, M. *Science* **2012**, *337*, 1521.
(8) (a) Nakashima, N.; Asakuma, S.; Kim, J.-M.; Kunitake, T. *Chem. Lett.* **1984**, *13*, 1709. (b) Yamada, T.; Ihara, H.; Ide, T.; Fukumoto, T.; Hirayama, C. *Chem. Lett.* **1984**, *13*, 1713.
(9) (a) Morin, J.-F. *Synlett* **2013**, *24*, 2032. (b) Xu, Y.; Smith, M. D.; Geer, M. F.; Pellechia, P. J.; Brown, J. C.; Wibowo, A. C.; Shimizu, L. S. *J. Am. Chem. Soc.* **2010**, *132*, 5334. (c) Hsu, T.-J.; Fowler, F. W.; Lauher, J. W. *J. Am. Chem. Soc.* **2012**, *134*, 142. (d) Rondeau-Gagné, S.; Neábo, J. R.; Desroches, M.; Larouche, J.; Brisson, J.; Morin, J.-F. *J. Am. Chem. Soc.* **2013**, *135*, 110. (e) Rondeau-Gagné, S.; Néabo, J. R.; Desroches, M.; Levesque, I.; Daigle, M.; Cantin, K.; Morin, J.-F. *Chem. Commun.* **2013**, *49*, 9546.
(10) Suzuki, M.; Comito, A.; Khan, S. I.; Rubin, Y. *Org. Lett.* **2010**, *12*, 2346.
(11) Topochemical polymerization of 1,3-dutadiynes: (a) Wegner, G. *Pure Appl. Chem.* **1977**, *49*, 443. (b) Matsumoto, A. *Polym. J.* **2003**, *35*, 93. (c) Sun, A.; Lauher, J. W.; Goroff, N. S. *Science* **2006**, *312*, 1030. (d) Lauher, J. W.; Fowler, F. W.; Goroff, N. S. *Acc. Chem. Res.* **2008**, *41*, 1215. (e) Neábo, J. R.; Rondeau-Gagné, S.; Vigier-Carriére, C.; Morin, J.-F. *Langmuir* **2013**, *29*, 3446. (f) Néabo, J. R.; Tohoundjona, K. I. S.; Morin, J.-F. *Org. Lett.* **2011**, *13*, 1358.
(12) (a) Hecht, S.; Khan, A. *Angew. Chem., Int. Ed.* **2003**, *42*, 6021. (b) Hashimoto, A.; Sogawa, H.; Shiotsuki, M.; Sanda, F. *Polymer* **2012**, *53*, 2559.
(13) Related studies and review on helical folding poly(*m*-phenylenediethynylene)s: (a) Suzuki, S.; Matsuura, K.; Nakazono, K.; Takata, T. *Polym. J.* **2014**, *46*, 355. (b) Suzuki, S.; Ishiwari, F.; Nakazono, K.; Takata, T. *Chem. Commun.* **2012**, *48*, 6478. (c) Yashima, E.; Maeda, K.; Iida, H.; Furusho, Y.; Nagai, K. *Chem. Rev.* **2009**, *109*, 6102.
(14) Nelson, J. C.; Saven, J. G.; Moore, J. S.; Wolynes, P. G. *Science* **1997**, *277*, 1793.
(15) Banno, M.; Yamaguchi, T.; Nagai, K.; Kaiser, C.; Hecht, S.; Yashima, E. *J. Am. Chem. Soc.* **2012**, *134*, 8718.
(16) Tobe, Y.; Utsumi, N.; Kawabata, K.; Nagano, A.; Adachi, K.; Araki, S.; Sonoda, M.; Hirose, K.; Naemura, K. *J. Am. Chem. Soc.* **2002**, *124*, 5350.
(17) Onouchi, H.; Okoshi, K.; Kajitani, T.; Sakurai, S.-i.; Nagai, K.; Kumaki, J.; Onitsuka, K.; Yashima, E. *J. Am. Chem. Soc.* **2008**, *130*, 229.
(18) Mio, M. J.; Prince, R. B.; Moore, J. S.; Kuebel, C.; Martin, D. C. *J. Am. Chem. Soc.* **2000**, *122*, 6134.
(19) Matsuda, K.; Stone, M. T.; Moore, J. S. *J. Am. Chem. Soc.* **2002**, *124*, 11836.
(20) Cai, M.; Mowery, M. D.; Menzel, H.; Evans, C. E. *Langmuir* **1999**, *15*, 1215.
(21) (a) Batchelder, D. N.; Evans, S. D.; Freeman, T. L.; Haeussling, L.; Ringsdorf, H.; Wolf, H. *J. Am. Chem. Soc.* **1994**, *116*, 1050. (b) Lim, C.; Sandman, D. J.; Sukwattanasinitt, M. *Macromolecules* **2008**, *41*, 675. (c) Koshihara, S.; Tokura, Y.; Takeda, K.; Koda, T.; Kobayashi, A. *J. Chem. Phys.* **1990**, *92*, 7581. (d) Shirai, E.; Urai, Y.; Itoh, K. *J. Phys. Chem. B* **1998**, *102*, 3765.
(22) Neumann, W.; Sixl, H. *Chem. Phys.* **1980**, *50*, 273.
(23) (a) Aida, T.; Tajima, K. *Angew. Chem., Int. Ed.* **2001**, *40*, 3803. (b) Néabo, J. R.; Vigier-Carriére, C.; Rondeau-Gagné, S.; Morin, J.-F. *Chem. Commun.* **2012**, *48*, 10144. (c) Wenz, G.; Muller, M. A.; Schmidt, M.; Wegner, G. *Macromolecules* **1984**, *17*, 837.

DOI: 10.1021/jacs.6b05582
J. Am. Chem. Soc. 2016, 138, 11001−11008